Computer-generated holography with ordinary display

OTOYA SHIGEMATSU[1], MAKOTO NARUSE[1], AND RYOICHI HORISAKI[1,*]

[1] *Department of Information Physics and Computing, Graduate School of Information Science and Technology, The University of Tokyo, 7-3-1 Hongo, Bunkyo-ku, Tokyo 113-8656, Japan*
[*] *Corresponding author: horisaki@g.ecc.u-tokyo.ac.jp*

Compiled December 15, 2023

We propose a method of computer-generated holography (CGH) using incoherent light emitted from a mobile phone screen. In this method, we suppose a cascade of holograms in which the first hologram is a color image displayed on the mobile phone screen. The hologram cascade is synthesized by solving an inverse problem with respect to the propagation of incoherent light. We demonstrate three-dimensional color image reproduction using a two-layered hologram cascade composed of an iPhone and a spatial light modulator.

http://dx.doi.org/10.1364/ao.XX.XXXXXX

Computer-generated holography (CGH) is a technique for synthesizing interference patterns in a computer to reproduce arbitrary optical fields. It has been studied for a long time in the field of optics and photonics [1]. Various applications of CGH have been proposed, such as laser processing and optical tweezers [2–4]. Among them, three-dimensional displays are a promising application of CGH for interface tools on next-generation virtual/augmented displays [5–10].

Most of the previous work on CGH has assumed spatially and temporally coherent light. This assumption is helpful in synthesizing holograms because numerical forward and backward propagations of coherent light can be calculated with a low computational cost using the fast Fourier transform [11]. However, laser sources for obtaining coherent light raise several issues in three-dimensional displays. Coherent light is not only harmful to the human eye but also causes speckle noise and zeroth-order light [12–14]. In addition, laser sources increase the cost and complexity of the display systems.

To address these issues, several studies have been conducted on holographic displays that utilize low-coherence light through techniques such as temporal multiplexing and the use of low-coherence light sources [15–20]. We recently demonstrated CGH using spatiotemporally incoherent light emitted from a white chip-on-board light-emitting diode, leveraging two spatial light modulators (SLMs) [21]. Nonetheless, employing two SLMs is impractical for real-world applications because of their high costs.

In this study, we introduce a more cost-effective and less complex method for practically implementing incoherent CGH. We achieve this by using an ordinary display device—specifically, a mobile phone screen in our experimental demonstration—in conjunction with a single SLM. Furthermore, unlike SLMs operating in amplitude mode, which can only display grayscale images, mobile phone screens have the capability to display color images. This capability enhances image reproduction performance in incoherent CGH.

The proposed method uses K holograms to reproduce Z layers of color images, as shown in Fig. 1. The ordinary screen device displays a color intensity image as the first hologram i_t, where $t \in \{1, 2, \ldots, T\}$ is the index of T color channels. T is three, which corresponds blue, green, and red, in most cases. The SLMs located downstream of the screen device display monochromatic real images h_k, where k is larger than 1. Here, $k \in \{1, 2, \ldots, K\}$ is the index of K holograms, where the first hologram is the color intensity image i_t, and holograms h_k from the second to Kth are of the amplitude-only or phase-only modulation type.

The kth hologram is translated to the complex amplitude field $v_{k,l}$ by the screen device or SLMs, depending on the wavelength λ_l of the lth spectral channel, where $l \in \{1, 2, \ldots, L\}$ is the index of the L spectral channels, as follows:

$$v_{k,l} = \begin{cases} \mathcal{P}_{l,t}[i_t] & (k = 1), & \textbf{(1)} \\ \mathcal{S}_{k,l}[h_k] & (k > 1). & \textbf{(2)} \end{cases}$$

$\mathcal{P}_{l,t}$ denotes an operator translating the color intensity image on the screen device to the complex amplitude field. $\mathcal{S}_{k,l}$ denotes an operator translating the monochromatic real images for the SLMs to the complex amplitude field.

The operator $\mathcal{P}_{l,t}$ for the first hologram on the screen device is expressed as

$$\mathcal{P}_{l,t}[i_t] = \left(\sum_{t=1}^{T} c_{l,t}^{\mathrm{disp}} \,\mathrm{samp}_{\uparrow}[i_t] \right)^{\frac{1}{2}}, \qquad \textbf{(3)}$$

where "$\mathrm{samp}_{\uparrow}$" is an operator for upsampling a low-resolution image to a high-resolution one for the propagation process and $c_{l,t}^{\mathrm{disp}}$ indicates the light amplitude of the lth spectral channel emitted from the tth color channel of the screen device. The operator $\mathcal{S}_{k,l}$ for the holograms from the second to Kth on the amplitude-modulation type or phase-modulation type SLMs is written as

$$\mathcal{S}_{k,l}[h_k] = \begin{cases} \mathrm{samp}_{\uparrow}[h_k] & (\text{for } k \in A), & \textbf{(4)} \\ \exp(j\Lambda_l \,\mathrm{samp}_{\uparrow}[h_k]) & (\text{for } k \in P), & \textbf{(5)} \end{cases}$$

where j is the imaginary unit, and Λ_l represents the spectral dispersion scaling factor, which is defined as $\Lambda_l = \lambda_L/\lambda_l$. A

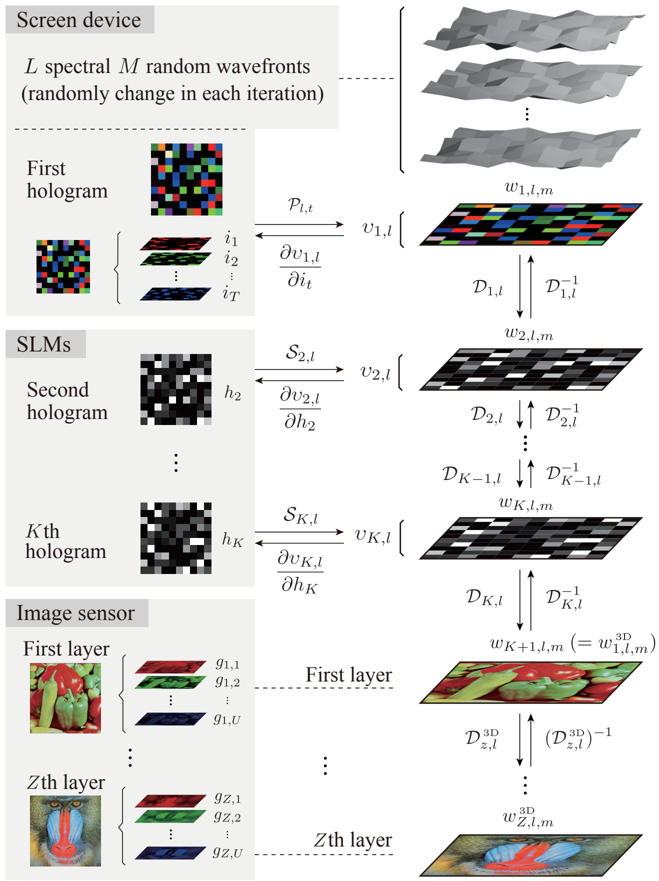

Fig. 1. The forward and backward propagation processes through a hologram cascade consisting of a color intensity hologram on the screen device and monochrome amplitude-only or phase-only holograms on the SLMs.

and P indicate sets of the indices of the amplitude-modulation type and phase-modulation type SLMs, respectively.

The forward propagation of incoherent light passing through the kth hologram is expressed as

$$w_{k+1,l,m} = \mathcal{D}_{k,l}[v_{k,l} w_{k,l,m}], \quad (6)$$

where $\mathcal{D}_{k,l}$ is an operator that represents the propagation from the kth hologram to the $k+1$th hologram, and $w_{k,l,m}$ is a complex amplitude field indicating the mth wavefront of the lth spectral channel just before the kth hologram. $m \in \{1, 2, \ldots, M\}$ is the index of M wavefronts, as described in Fig. 1, where the incoherent light propagation is described with a set of random wavefronts [20].

Wavefronts $w_{K+1,l,m}$ after passing through the holographic cascade propagate from the first layer to the zth layer in the observation space and are described as

$$w^{3D}_{z,l,m} = \mathcal{D}^{3D}_{z,l}[w_{K+1,l,m}], \quad (7)$$

where $\mathcal{D}^{3D}_{z,l}$ is an operator for the propagation from the first layer to the zth layer, and $w^{3D}_{z,l,m}$ is a complex amplitude field representing the mth wavefront of the lth spectral channel at the zth layer. $z \in \{1, 2, \ldots, Z\}$ is the index of Z layers in the observation space. The color intensity image $g_{z,u}$ of the uth color channel at the zth layer is observed as

$$g_{z,u} = \frac{1}{M} \sum_{l=1}^{L} c^{\text{cam}}_{u,l} \sum_{m=1}^{M} |w^{3D}_{z,l,m}|^2, \quad (8)$$

where $c^{\text{cam}}_{u,l}$ indicates the sensitivity of the lth spectral channel to the uth color channel on a color image sensor. $u \in \{1, 2, \ldots, U\}$ is the index of U color channels of the color image sensor, and U is three (blue, green, and red) in most cases.

Our aim is to obtain $i_1, i_2, \cdots, i_T$ and $h_2, h_3, \cdots, h_K$ that bring $g_{z,u}$ closest to the target color intensity images $\hat{g}_{z,u}$ of the uth color channel at the zth layer. Therefore, this inverse problem is written as

$$\mathop{\arg\min}_{i_1,\cdots,i_T,h_2,\cdots,h_K} \; e \quad (9)$$

$$e = \sum_{z=1}^{Z} \sum_{u=1}^{U} \| g_{z,u} - \hat{g}_{z,u} \|_2^2 , \quad (10)$$

where e is the cost function for synthesizing the holograms and $\| \bullet \|_2$ denotes the ℓ_2 norm.

The inverse problem of Eq. (9) is solved in the framework of stochastic gradient descent based on the compressive propagation [20]. The partial derivatives of the cost function e with respect to i_t and h_k are respectively written with the chain rule as follows:

$$\frac{\partial e}{\partial i_t} = \sum_{l=1}^{L} \frac{\partial v_{1,l}}{\partial i_t} \cdot \frac{\partial e}{\partial v_{1,l}}, \quad (11)$$

$$\frac{\partial e}{\partial h_k} = \sum_{l=1}^{L} \frac{\partial v_{k,l}}{\partial h_k} \cdot \frac{\partial e}{\partial v_{k,l}} \quad (\text{for } k > 1). \quad (12)$$

The partial derivative of the second term on the right side of Eqs. (11) and (12) is calculated as

$$\frac{\partial e}{\partial v_{k,l}} = \frac{4}{M} \sum_{z=1}^{Z} \sum_{m=1}^{M} w^{*}_{k,l,m} \mathcal{D}^{-1}_{k,l} [v^{*}_{k+1,l} \mathcal{D}^{-1}_{k+1,l} [\cdots [v^{*}_{K,l} \mathcal{D}^{-1}_{K,l} [(\mathcal{D}^{3D}_{z,l})^{-1} [w^{3D}_{z,l,m} \sum_{u=1}^{U} c^{\text{cam}}_{u,l} (g_{z,u} - \hat{g}_{z,u})]]] \cdots]], \quad (13)$$

where $\mathcal{D}^{-1}_{k,l}$ and $(\mathcal{D}^{3D}_{z,l})^{-1}$ are operators for the inverse propagation of $\mathcal{D}_{k,l}$ and $\mathcal{D}^{3D}_{z,l}$, respectively. The superscript $*$ denotes the complex conjugate.

The partial derivative of the left side of Eq. (11) is written as

$$\frac{\partial e}{\partial i_t} = \sum_{l=1}^{L} \text{real} \left[\text{samp}_{\downarrow} \left[\frac{c^{\text{disp}}_{l,t}}{2 v_{1,l}} \frac{\partial e}{\partial v_{1,l}} \right] \right], \quad (14)$$

where "real" denotes the real part of the complex amplitude, and "$\text{samp}_{\downarrow}$" is an operator for downsampling. The partial derivative on the left side of Eq. (12) is calculated as the following two cases depending on whether the kth hologram is the amplitude-modulation or phase-modulation type:

$$\frac{\partial e}{\partial h_k} = \begin{cases} \sum_{l=1}^{L} \text{real} \left[\text{samp}_{\downarrow} \left[\frac{\partial e}{\partial v_{k,l}} \right] \right] & (\text{for } k \in A), \quad (15) \\ \sum_{l=1}^{L} \text{real} \left[\text{samp}_{\downarrow} \left[-j \Lambda_l v^{*}_{k,l} \frac{\partial e}{\partial v_{k,l}} \right] \right] & (\text{for } k \in P). \quad (16) \end{cases}$$

The color intensity hologram i_t on the screen device and monochrome amplitude-only or phase-only holograms on the

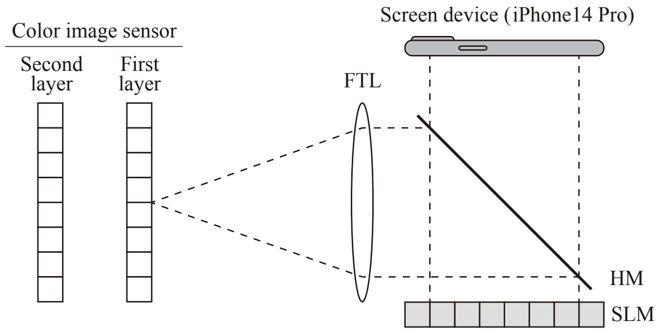

Fig. 2. Experimental optical setup of FourierCGH. The first color hologram was displayed on an iPhone 14 Pro, and the second hologram was displayed on a reflective phase-modulation type SLM. FTL: Fourier transform lens and HM: half mirror. Note that the FTL was removed for FresnelCGH.

SLMs are updated by the following gradient descent process based on the Adam optimizer [22]:

$$i_t \leftarrow i_t - \text{Adam}\left[\frac{\partial e}{\partial i_t}\right], \quad \textbf{(17)}$$

$$h_k \leftarrow h_k - \text{Adam}\left[\frac{\partial e}{\partial h_k}\right] \quad (\text{for } k > 1), \quad \textbf{(18)}$$

where "Adam" is an operator for the Adam optimizer that calculates the updating step using the derivatives. The random wavefronts $w_{1,l,m}$ just before the first hologram randomly change in each iteration for the compressive propagation of incoherent light by stochastic gradient descent, as shown in Fig. 1 [20].

In this study, we experimentally demonstrated the proposed method based on Fourier transform CGH and Fresnel propagation CGH, which are refereed to as FourierCGH and FresnelCGH, respectively. FourierCGH employed the Fourier transform lens (FTL) after the Kth hologram. An FTL has been used in CGH for enhancing the spatial resolution of the propagation space by means of the optical Fourier transform [11]. On the other hand, FresnelCGH does not use an FTL, and its optical setup is thus more compact than that of FourierCGH.

The optical setup for the FourierCGH experiment is shown in Fig. 2. The setup was a two-layered hologram cascade, and so $K = 2$. The screen device was an iPhone (iPhone 14 Pro manufactured by Apple, pixel count: 2556 × 1179, pixel pitch: 55.2 µm). Incoherent light with three color channels ($T = 3$) emitted from the iPhone was reflected by a phase-modulation type SLM (X13138 manufactured by Hamamatsu Photonics, pixel count: 1272 × 1024, pixel pitch: 12.5 µm) located at a distance of 12 cm from the iPhone. The reflected light was Fourier transformed by the FTL with a focal length f of 15 cm. Different color images were reproduced at the focal plane of the FTL and 1.5 cm away from the focal plane, then $Z = 2$, and these were observed with a color image sensor ($U = 3$, DFK38UX304 manufactured by The Imaging Source, pixel count: 4096 × 3000, pixel pitch: 3.45 µm).

In the numerical propagation process, the number of spectral channels L was 3, and their wavelengths λ_l were set to $\lambda_1 =$ 460 nm, $\lambda_2 = 535$ nm, and $\lambda_3 = 625$ nm. This condition was determined by measuring the spectrum of a white image displayed on the iPhone with a spectrometer (CCS100 manufactured by Thorlabs). The transform matrices between color and spectral channels $c^{\text{disp}}_{l,t}$ and $c^{\text{cam}}_{u,l}$ were set to be identity matrices.

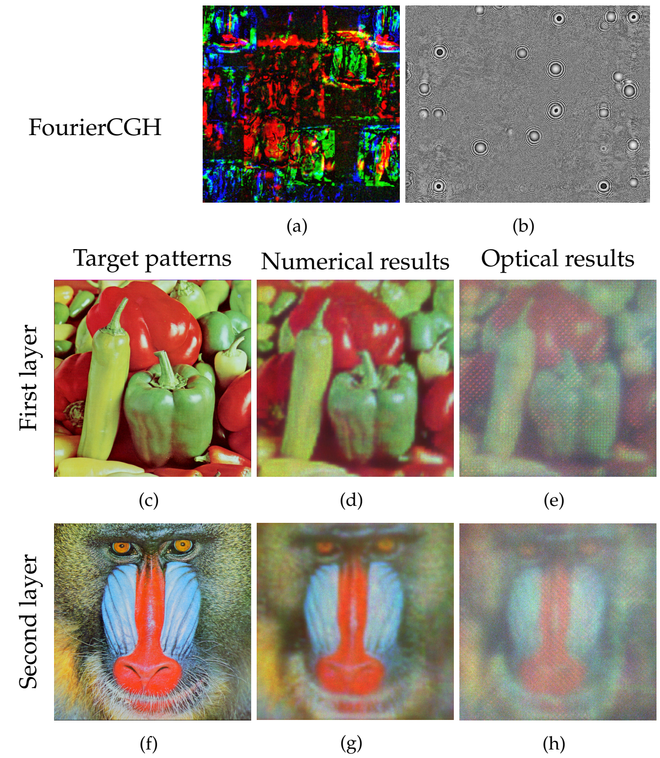

Fig. 3. Results of three-dimensional color image reproduction of FourierCGH. (a) Color intensity hologram on the iPhone and (b) phase-only hologram on the SLM, which is normalized in the interval $[-\pi, \pi]$. Target color images of the (c) first and (f) second layers. Numerical reproductions of the (d) first and (g) second layers. Optical reproductions of the (e) first and (h) second layers.

On the color intensity hologram i_t, the pixel pitch and the pixel count were set to 55.2 µm and 224^2. On the phase-only hologram h_K, the pixel pitch and the pixel count were set to 12.5 µm and 1272 × 1024. On the wavefronts $w_{k,l,m}$ propagating through the holographic cascade, the pixel pitch d and the pixel count Q^2 were set to 12 µm and 2048^2. In FourierCGH, the propagation operator $\mathcal{D}_{K,l}$ after the Kth hologram was that for Fraunhofer diffraction, which corresponded to the Fourier transform, and the other propagation operators were those for Fresnel diffraction. Then, the pixel pitch of the observation space of FourierCGH was calculated as $\lambda_l f / Qd$ [11]. To compensate the wavelength-dependent pixel pitch, each color channel of the target image was downsized by a factor of λ_1 / λ_l. All the holograms and the target images were set to the central regions on the layers. In the optimization process, the number of random wavefronts M was set to 20. The learning rate of the Adam optimizer was set to 0.1, and the other parameters were the same as those in the original work [22]. The number of iterations was 1500.

The numerical and experimental results of FourierCGH are shown in Fig. 3. We assumed the standard color images of *peppers* and *mandrill* for the target images on the first and second layers, as shown in Figs. 3(c) and 3(f), respectively. The color intensity hologram and the phase-only hologram were synthesized as shown in Figs. 3(a) and 3(b). These holograms were displayed on the iPhone and the SLM. The numerical reproductions on the first and second layers are shown in Figs. 3(d) and 3(g), respectively. The number of random wavefronts was

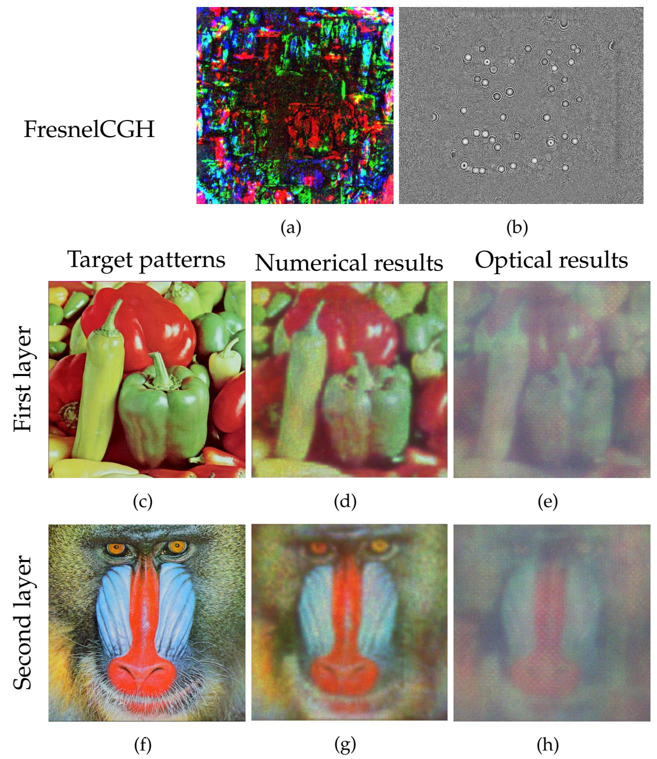

Fig. 4. Results of three-dimensional color image reproduction of FresnelCGH. (a) Color intensity hologram on the iPhone, and (b) phase-only hologram on the SLM, which is normalized in the interval $[-\pi, \pi]$. Target color images of the (c) first and (f) second layers. Numerical reproductions of the (d) first and (g) second layers. Optical reproductions of the (e) first and (h) second layers.

set to 300 for the final reproduction. The peak signal-to-noise ratios (PSNRs) of the blue, green, and red channels between the target and reproduced images on the first layer were 21.0 dB, 20.3 dB, and 20.4 dB, respectively. Those on the second layer were 17.6 dB, 18.0 dB, and 18.5 dB, respectively. The optical reproductions on the first and second layers are shown in Figs. 3(e) and 3(h), respectively, where speckle noise and zeroth-order light were not observable. Visualization 1 provides a continuous transition in optical reproduction from the first layer to the second layer. The pixel count of these optically reproduced images was 1250^2 on the image sensor. Those results show the promising performance of three-dimensional color image reproduction with incoherent FourierCGH using the iPhone.

The numerical and experimental results of FresnelCGH are shown in Fig. 4. The FTL in Fig. 2 was removed for FresnelCGH. The distance between the SLM in the holographic cascade and the first layer in the observation space was set to 15 cm. The other optical and optimization conditions were the same as those in FourierCGH. In FresnelCGH, all of the propagation operators corresponded to Fresnel diffraction. The target color images on the first and second layers are shown in Figs. 4(c) and 4(f), respectively, which were identical to those in FourierCGH. The numerical reproductions on the first and second layers are shown in Figs. 4(d) and 4(g). The PSNRs of the blue, green, and red channels on the first layer were 18.9 dB, 18.9 dB, and 19.6 dB. Those on the second layer were 16.1 dB, 17.7 dB, and 18.0 dB. The optical reproductions on the first and second layers are shown in Figs. 4(e) and 4(h), respectively. Visualization 2 provides a continuous transition in optical reproduction from the first layer to the second layer. Those results showed that the reproduction performance of FresnelCGH was slightly worse than that of FourierCGH due to the improvement of the diffraction efficiency by the FTL. However, the optical setup of FresnelCGH is compact compared with that of FourierCGH.

In summary, we proposed and demonstrated a CGH method utilizing incoherent light emitted from an ordinary screen device, like those integrated into widely available mobile phones. We modeled spatiotemporally incoherent light propagating through a holographic cascade, where the first hologram was the color intensity image on the screen device. Then, we synthesized the holographic cascade for three-dimensional color image reproduction by using stochastic gradient descent based on compressive propagation. The performance of the proposed method was numerically and experimentally verified based on both FourierCGH and FresnelCGH using an iPhone and a phase-modulation type SLM. Our method simplifies optical setups for CGH and realizes a high holographic reproduction performance. Therefore, it is promising for visual interfaces in next-generation augmented/virtual reality.

Funding. Japan Society for the Promotion of Science (JP20K05361, JP20H05890, JP23H01874, JP23H05444); Asahi Glass Foundation.

Disclosures. The authors declare no conflicts of interest.

Data availability. Data may be obtained from the authors upon reasonable request.

REFERENCES

1. K. Matsushima, *Introduction to Computer Holography: Creating Computer-Generated Holograms as the Ultimate 3D Image* (Springer Nature, 2020).
2. P. S. Salter and M. J. Booth, Light. Sci. & Appl. **8**, 110 (2019).
3. Y. Yang, Y.-X. Ren, M. Chen, Y. Arita, and C. Rosales-Guzmán, Adv. Photonics **3**, 034001 (2021).
4. J. Gieseler, J. R. Gomez-Solano, A. Magazzù, I. P. Castillo, L. P. García, M. Gironella-Torrent, X. Viader-Godoy, F. Ritort, G. Pesce, A. V. Arzola *et al.*, Adv. Opt. Photonics **13**, 74 (2021).
5. J.-H. Park, J. Inf. Disp. **18**, 1 (2017).
6. E. Sahin, E. Stoykova, J. Mäkinen, and A. Gotchev, ACM Comput. Surv. (CSUR) **53**, 1 (2020).
7. P.-A. Blanche, Light. Adv. Manuf. **2**, 446 (2021).
8. D. Pi, J. Liu, and Y. Wang, Light. Sci. & Appl. **11**, 231 (2022).
9. Z. He, X. Sui, G. Jin, and L. Cao, Appl. Opt. **58**, A74 (2019).
10. J. Xiong, E.-L. Hsiang, Z. He, T. Zhan, and S.-T. Wu, Light. Sci. & Appl. **10**, 216 (2021).
11. J. W. Goodman, *Introduction to Fourier optics* (W. H. Freeman and Company, 2017).
12. K. V. Chellappan, E. Erden, and H. Urey, Appl. Opt. **49**, F79 (2010).
13. T. Shimobaba and T. Ito, Opt. Express **23**, 9549 (2015).
14. J. Liang, S.-Y. Wu, F. K. Fatemi, and M. F. Becker, Appl. Opt. **51**, 3294 (2012).
15. Y. Takaki and M. Yokouchi, Opt. Express **19**, 7567 (2011).
16. S. Lee, D. Kim, S.-W. Nam, B. Lee, J. Cho, and B. Lee, Sci. Reports **10**, 18832 (2020).
17. Y. Peng, S. Choi, J. Kim, and G. Wetzstein, Sci. Adv. **7**, eabg5040 (2021).
18. B. Lee, D. Kim, S. Lee, C. Chen, and B. Lee, Sci. Reports **12**, 2811 (2022).
19. N. Barré and A. Jesacher, Opt. Lett. **47**, 425 (2022).
20. R. Horisaki, T. Aoki, Y. Nishizaki, A. Röhm, N. Chauvet, J. Tanida, and M. Naruse, Opt. Lett. **47**, 613 (2022).
21. R. Suda, M. Naruse, and R. Horisaki, Opt. Lett. **47**, 3844 (2022).
22. D. P. Kingma, J. Ba, Y. Bengio, and Y. LeCun, ICLR, San Diego (2015).

FULL REFERENCES

1. K. Matsushima, *Introduction to Computer Holography: Creating Computer-Generated Holograms as the Ultimate 3D Image* (Springer Nature, 2020).
2. P. S. Salter and M. J. Booth, “Adaptive optics in laser processing,” Light. Sci. & Appl. **8**, 110 (2019).
3. Y. Yang, Y.-X. Ren, M. Chen, Y. Arita, and C. Rosales-Guzmán, “Optical trapping with structured light: a review,” Adv. Photonics **3**, 034001–034001 (2021).
4. J. Gieseler, J. R. Gomez-Solano, A. Magazzù, I. P. Castillo, L. P. García, M. Gironella-Torrent, X. Viader-Godoy, F. Ritort, G. Pesce, A. V. Arzola *et al.*, “Optical tweezers—from calibration to applications: a tutorial,” Adv. Opt. Photonics **13**, 74–241 (2021).
5. J.-H. Park, “Recent progress in computer-generated holography for three-dimensional scenes,” J. Inf. Disp. **18**, 1–12 (2017).
6. E. Sahin, E. Stoykova, J. Mäkinen, and A. Gotchev, “Computer-generated holograms for 3d imaging: a survey,” ACM Comput. Surv. (CSUR) **53**, 1–35 (2020).
7. P.-A. Blanche, “Holography, and the future of 3d display,” Light. Adv. Manuf. **2**, 446–459 (2021).
8. D. Pi, J. Liu, and Y. Wang, “Review of computer-generated hologram algorithms for color dynamic holographic three-dimensional display,” Light. Sci. & Appl. **11**, 231 (2022).
9. Z. He, X. Sui, G. Jin, and L. Cao, “Progress in virtual reality and augmented reality based on holographic display,” Appl. Opt. **58**, A74–A81 (2019).
10. J. Xiong, E.-L. Hsiang, Z. He, T. Zhan, and S.-T. Wu, “Augmented reality and virtual reality displays: emerging technologies and future perspectives,” Light. Sci. & Appl. **10**, 216 (2021).
11. J. W. Goodman, *Introduction to Fourier optics* (W. H. Freeman and Company, 2017).
12. K. V. Chellappan, E. Erden, and H. Urey, “Laser-based displays: a review,” Appl. Opt. **49**, F79–F98 (2010).
13. T. Shimobaba and T. Ito, “Random phase-free computer-generated hologram,” Opt. Express **23**, 9549–9554 (2015).
14. J. Liang, S.-Y. Wu, F. K. Fatemi, and M. F. Becker, “Suppression of the zero-order diffracted beam from a pixelated spatial light modulator by phase compression,” Appl. Opt. **51**, 3294–3304 (2012).
15. Y. Takaki and M. Yokouchi, “Speckle-free and grayscale hologram reconstruction using time-multiplexing technique,” Opt. Express **19**, 7567–7579 (2011).
16. S. Lee, D. Kim, S.-W. Nam, B. Lee, J. Cho, and B. Lee, “Light source optimization for partially coherent holographic displays with consideration of speckle contrast, resolution, and depth of field,” Sci. Reports **10**, 18832 (2020).
17. Y. Peng, S. Choi, J. Kim, and G. Wetzstein, “Speckle-free holography with partially coherent light sources and camera-in-the-loop calibration,” Sci. Adv. **7**, eabg5040 (2021).
18. B. Lee, D. Kim, S. Lee, C. Chen, and B. Lee, “High-contrast, speckle-free, true 3d holography via binary cgh optimization,” Sci. Reports **12**, 2811 (2022).
19. N. Barré and A. Jesacher, “Holographic beam shaping of partially coherent light,” Opt. Lett. **47**, 425–428 (2022).
20. R. Horisaki, T. Aoki, Y. Nishizaki, A. Röhm, N. Chauvet, J. Tanida, and M. Naruse, “Compressive propagation with coherence,” Opt. Lett. **47**, 613–616 (2022).
21. R. Suda, M. Naruse, and R. Horisaki, “Incoherent computer-generated holography,” Opt. Lett. **47**, 3844–3847 (2022).
22. D. P. Kingma, J. Ba, Y. Bengio, and Y. LeCun, “3rd international conference on learning representations,” ICLR, San Diego (2015).